Nature Environment and Pollution Technology
An International Quarterly Scientific Journal

p-ISSN: 0972-6268
(Print copies up to 2016)
e-ISSN: 2395-3454

Vol. 23 | No. 2 | pp. 591-604 | 2024

Original Research Paper

https://doi.org/10.46488/NEPT.2024.v23i02.001

Open Access Journal

Assessment of Deposited Red Clay Soil in Kirkuk City Using Remote Sensing Data and GIS Techniques

V. F. Salahalden†, M. A. Shareef and Q. A. M. Al Nuaimy
Surveying, Engineering Technical College-Kirkuk, Northern Technical University, Mosul, Iraq
†Corresponding author: V. F. Salahalden; veyan.farhad @ntu.edu.iq

Nat. Env. & Poll. Tech.
Website: www.neptjournal.com

Received: 06-09-2023
Revised: 01-11-2023
Accepted: 09-11-2023

Key Words:
Red clay soil
Remote sensing
GIS
IDW
Linear regression model

ABSTRACT

This study investigates the physical characteristics of red clay using the IDW approach and linear regression modeling in an area of 268.12 km^2, focusing on Kirkuk, Bor, and Jambor structures. Through the analysis of 52 soil samples and the integration of laboratory data with IDW and regression results, several significant findings have emerged. The IDW method combined with linear regression proves to be a cost-effective and efficient approach for obtaining soil property data and generating accurate digital maps of red clay's physical features. The Silt concentration exhibits a wide range, while the gravel content remains relatively low, indicating the predominance of silt in the soil composition. Analysis of Atterberg limits reveals the soil's behavior and consistency in response to moisture, with the plasticity index generally falling within the low to medium range due to the considerable silt content in most soil samples. The linear regression model highlights positive correlations between the liquid limit, plastic limit, and plasticity index. Moderately positive relationships exist between the liquid limit and clay content, as well as a weak positive association between the liquid limit and specific gravity. Dry density, on the other hand, shows no significant correlation with other physical variables, suggesting its independence from the measured parameters. The plastic limit demonstrates a stronger relationship with the clay content compared to the liquid limit. Additionally, weak positive correlations are found between the liquid limit, plastic limit, and specific gravity and water content, indicating the influence of moisture on these parameters. Furthermore, gravel exhibits a moderate positive correlation with sand and silt concentrations, while a strong positive correlation is observed between sand and silt contents, underscoring their close association with the soil composition.

INTRODUCTION

In the field of soil science, the formation of "red clay," an insoluble clay mineral, occurs through the weathering of rocks in the Earth's crust under wet and warm weather conditions (Yang et al. 2020a, Zhang et al. 2020). Soil, which comprises physical and chemical properties, mineral particles, organic components, air, and water, plays a vital role in the natural environment (Taqi et al. 2016). The particle size distribution of soil is an important physical property and is typically categorized into three fractions: clay (0.002 mm), silt (0.002-0.02 mm), and sand (>0.02 mm) (Fongaro et al. 2018).

Traditional soil surveys provide valuable information on the physical and chemical characteristics of soil at the component level, enabling the creation of maps that illustrate the spatial distribution of these characteristics across different locations (Zhu et al. 2010). However, mapping soil properties can be challenging in areas with low agricultural potential, and conventional soil survey methods can be time-consuming and expensive, particularly in remote regions (Shareef & Hasan 2020).

Many techniques have been proposed in recent decades to estimate various soil parameters using remote sensing data (Mohamed et al. 2020). In addition to providing information about the spatiotemporal variations in soil, remote sensing (RS) and GIS techniques offer dependable alternatives to older approaches that can cover large areas (Akumu et al. 2015, Jaber et al. 2022, Mezaal & Pradhan 2018, Mezaal et al. 2018, 2017a, 2017b, Shafri, et al. 2017, Sahbeni et al. 2023). RS provides spatial and integrated images of land attributes, enabling a comprehensive understanding of the landscape. By combining multispectral high-resolution data with digital image processing methods, remote sensing can enhance the identification of lithology and geological formations (Martins & Gadiga 2015).

Moreover, remote sensing data can serve as supporting variables for predicting surface soil texture across geographic

areas with the collection of a limited number of soil samples (Liao et al. 2013). Regression analysis models and geostatistical approaches are commonly used to estimate soil properties from RS data (da Silva Chagas et al. 2016, Sridevy et al. 2023). Geographic information systems (GIS) are employed to organize, analyze, and store the extracted information in databases. GIS also facilitates the modeling and mapping of soil properties by utilizing interpolation methods to depict the spatial distribution of the data (Maarez et al. 2022). GIS is used to model and map soil properties and the location distribution of the extracted data using interpolation methods (Akumu et al. 2015).

However, factors such as soil heterogeneity, interpolation method, and sampling can influence the quality of maps generated through geostatistical techniques (Shareef et al. 2020). Spatial interpolation techniques, which consider the actual locations of sample data points, are widely employed to produce maps by quantifying assessments for researched parameters across various positions. These techniques involve the weighted averaging of surrounding data points (Raheem et al. 2022, 2023, Raheem & Omar 2021). Collecting soil data is crucial for addressing queries related to natural hazards, land management, and reconstruction (Buenemann et al. 2023)

Given the absence of a precise map indicating the physical characteristics and distribution of Kirkuk's red clay, this study utilized GIS-based linear regression models to assess and map the physical characteristics of red clay. However, due to time constraints and the unpredictable nature of soil deposits, gathering and interpreting data on soil physical parameters with high precision is challenging. Hence, the primary objective of this study is to identify the most reliable correlations among indicators of clay soil properties, employing the ordinary least squares method to describe these relationships.

MATERIAL AND METHODS

Location and Geologic Setting of the Study Area

The research site is located in the northern part of Iraq, specifically within a longitude range of 44° 00' to 44° 50′ E and a latitude range of 35′ 10′ to 35′ 40′ N (Fig. 1). The study area covers a substantial area of 268.12 km2 and encompasses the Fatha and Injana formations. The climate in this region can be characterized as semiarid and Mediterranean, with hot and dry summers and cold winters. The majority of rainfall occurs between December and March, while the summer months experience little to no precipitation (Muhaimeed & Al-Hedny 2013).

Topography and Geology of the Study Area

The city of Kirkuk is situated in the hilly northern part of the Kirkuk Plain, with an elevation ranging from 340 to 360 meters above sea level. The Kirkuk structure, also known as

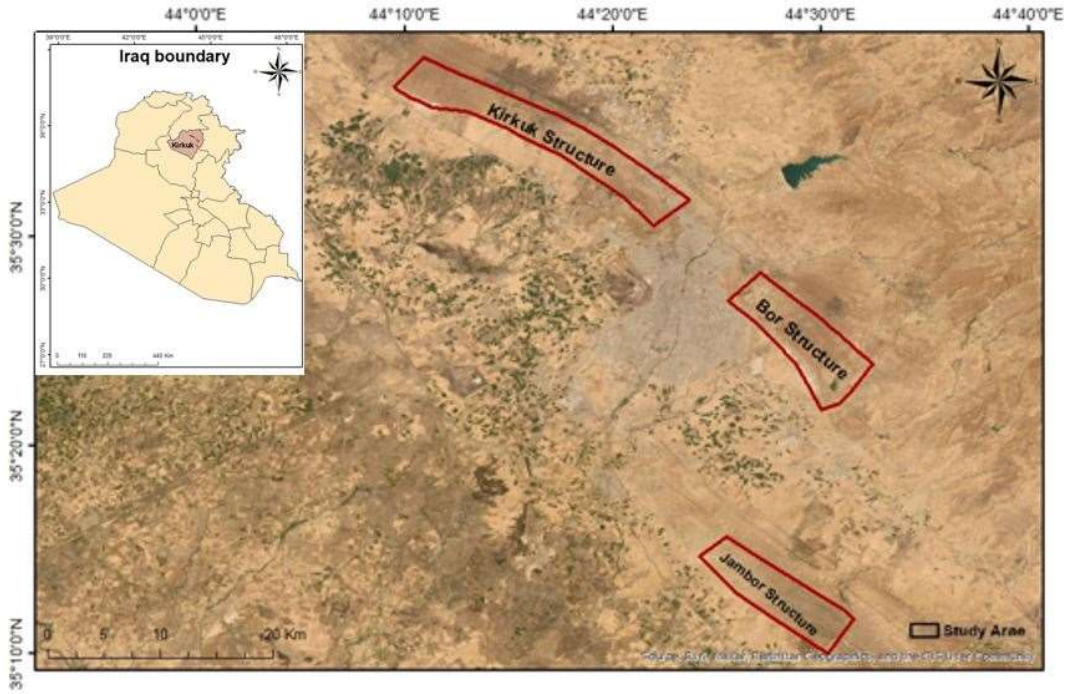

Fig. 1: Location map of the study area.

Baba Dome, marks the northern edge of the plain, while the Hamrin structure delineates the eastern edge. The western and northern margins are outlined by the Hamrin structure and the lower Zap River, respectively (Buday 1980).

During the Pliocene epoch, significant tectonic movements led to the formation of various structures in the region, including Kirkuk, Bia-Hassan, Khabaze, Jambur, and Hamrin, as well as a broad syncline represented by the Kirkuk-Hawija plain. The erosion caused by the rocks in the highest areas between these structures resulted in the deposition of eroded materials from higher grounds to lower areas (Jassim & Goff 2006). In Kirkuk, the earliest rocks belong to the Fatha Formation, which originated in the middle Miocene. This formation consists of gypsum, red claystone, and green marl, overlain by sandstone and red claystone from the Injana Formation, which dates back to the Upper Miocene (Al-Naqib 1959).

The research region is predominantly flat, with some variations in elevation primarily concentrated in the southwestern corner. The presence of anticlines such as Bor, Jambor, and Kirkuk indicates that the high terrain resulted from structural forces. The elevation in the surveyed area ranges from 500 meters above sea level in the northeast to 200 meters above sea level in the southwest (Jabbar 2015). The Fatha Formation, originating from the middle Miocene epoch, is exposed in the study area. It comprises thick gypsum layers alternating with reddish-brown or green claystone, marl, or limestone, with a thickness range of 100 to 200 meters (Jabbar 2015). The Injana Formation, composed of thin-bedded calcareous sandstone, red and green mudstone, and siltstone, was formed later in the Miocene period (Alhirmizy 2015).

Methods

The methodology employed in this study encompasses field measurements, satellite data analysis, and the application of geographic information systems (GIS) techniques. Specifically, inverse distance weighting (IDW) and a linear regression model were utilized to investigate the distribution of red clay and various physical properties of the soil. The physical properties considered in this analysis include soil texture, Atterberg limits, specific gravity, dry density, and water content. A graphical representation of the overall methodology can be found in Fig. 2.

Field measurements and soil analysis: A total of fifty-two soil sampling sites were selected within the Bor, Jambor, and

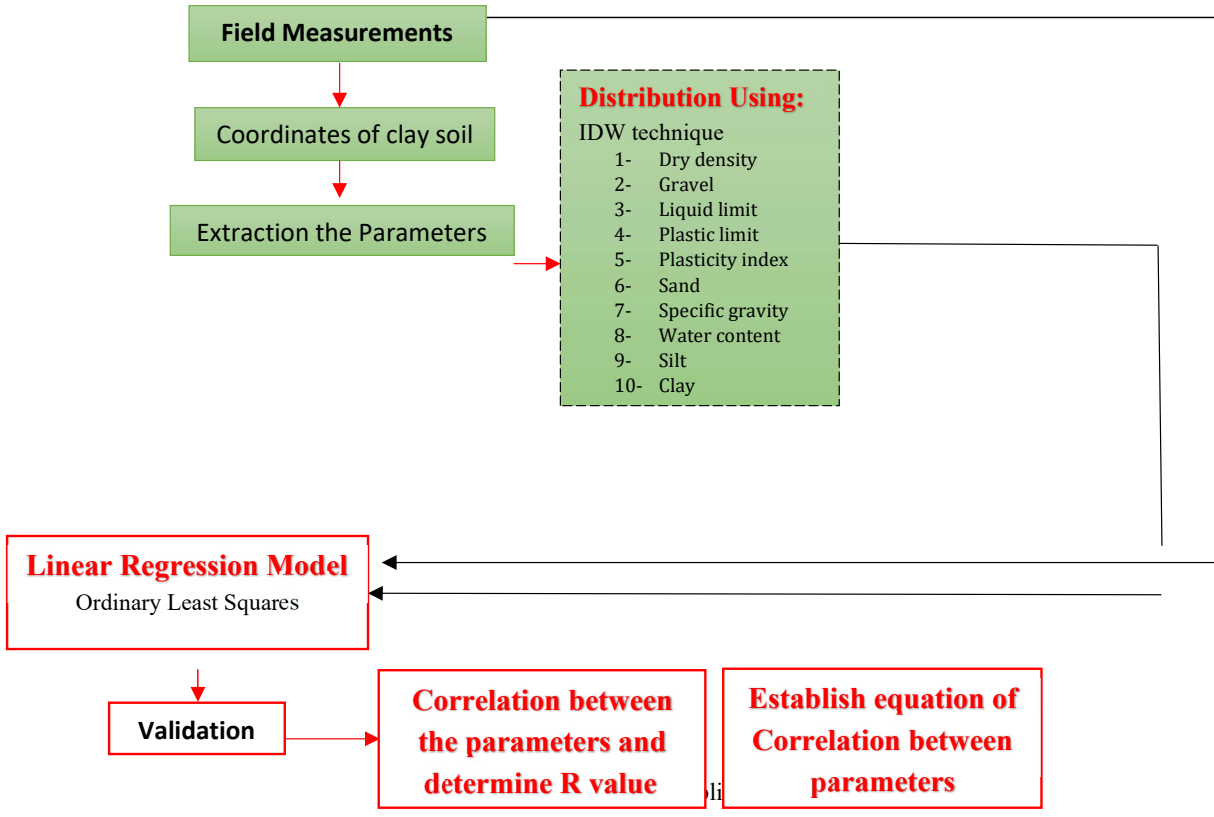

Fig. 2: Flow chart of the applied method.

Kirkuk structures, which are part of the Fatha and Injana Formations. The precise coordinates of these sites were determined using a portable GPS device with an accuracy of ±3.6. For the analysis of soil properties, an HS-5001EZ moisture-density meter was employed to measure the dry density and water content. At each sampling site, soil samples were collected at a depth of 30 cm after removing the topsoil layer. These samples were then air-dried before being transported to the laboratory for further analysis.

In the laboratory, the soil samples underwent various tests to determine their physical properties. The Atterberg limits, which include the liquid limit (LL) and plastic limit (PL), were determined using the Casagrande three-point approach. The specific gravity of the soil was measured, and the percentages of sand, silt, and clay in the soil were determined using hydrometers. The liquid limits were calculated based on the 3-millimeter diameter of the soil thread during the testing for plastic limits (Zolfaghari et al. 2015). All measurements and analyses were conducted following the standards set by the American Society for Testing and Materials (ASTM)

Inverse distance weighted: Geostatistics is a statistical branch that specializes in the analysis of spatial distribution and variability(Shit et al. 2016, Yadav et al. 2023). In this study, the spatial patterns of various physical properties of red clay were described using interpolated maps created through the inverse distance weighted (IDW) method (Belief 2018, Ratshiedana et al. 2023). The IDW interpolation approach was utilized to predict the values of unmeasured sites or unsampled locations (Shit et al. 2016). Geographers often employ the IDW interpolation technique to fill in data gaps, where it uses a weighted combination of nearby sample points to estimate values in grid cells. The closer the data points are to the target location, the greater their influence on the estimation process (Nistor et al. 2020, Zhang et al. 2020).

To determine the unknown value, Z(X), at a specific position X, the following equations, Eq. 1 and Eq. 2, were employed:

$$Z(X) = \sum_{i=1}^{N} W_I \, Z(X_I), \quad \ldots(1)$$

where n represents the monitoring station, Z(X) represents the value at the sampled sites, and W_I represents the weight of X_I, which is defined as:

$$W_I = \frac{\frac{1}{d_j^k}}{\left(\sum_{i=1}^{n} \frac{1}{d_j^k}\right)} \quad \ldots(2)$$

where d_i is the horizontal distance between the interpolation points and the observed positions, and k is the distance power (Yang et al. 2020b).

Linear Regression Model

Simple regression analysis is a statistical tool that explores the relationships between dependent and independent variables by employing various regression models, including linear regression, exponential regression, logarithmic regression, polynomial regression, and power regression models (Eskandari et al. 2023, Shahien & Ogila 2022). The assessment of regression relationships often involves the use of Pearson's correlation coefficient. By calculating Pearson's correlation coefficient (R), we can evaluate the strength and direction of the association between two variables. In the matrix plot, we observed strong correlations (R = 0.68), moderate correlations (R = 0.36–0.67), and weak correlations (R = -0.35) between the variables (Shahien & Ogila 2022).

The function of linear regression is given in Eq. 3:

$$Y = A + BX + \mathcal{E} \text{ (Shareef et al. 2014)} \quad \ldots(3)$$

Where Y is the dependent variable, X is the independent variable, A is the intercept, B is the slope, and $\mathcal{E}$ is the error term.

RESULTS AND DISCUSSION

Field measurements of soil were conducted at 52 selected locations within the city of Kirkuk, specifically in three sections: the Bor, Jambor, and Kirkuk structures. The HS-5001EZ moisture-density gauge was utilized for this purpose.

Laboratory and Statistical Analysis

Particle size analysis: Upon conducting a specific size analysis of the fifty-two soil samples, it was observed that the percentage of gravel was generally low across most samples, ranging from 0 to 4 percent. However, there was one site in the Kirkuk structure's Injana Formation where the percentage of gravel was notably higher at 16.3 percent. On average, the gravel content was 0.49 percent in the Injana Formation and slightly higher at 0.66 percent in the Fatha Formation.

The results for sand content varied from 0 to 30 percent, with two locations in the Injana Formation exhibiting higher percentages of 42 and 61 percent. In contrast, the average sand content in the Fatha Formation was 7.5 percent, slightly lower than the average of 8.9 percent in the Injana Formation. Silt, on the other hand, predominated in the vast majority of the soil samples, although specific percentages were not provided in the given information.

Atterberg limits: The Atterberg limits were used to determine the boundary between different physical states of sediments. The findings of the Atterberg limits analysis revealed that the liquid limit ranged from 18 to 43%, with an average of 30.17%. Within the Jambor structure, the Fatha Formation exhibited the highest percentage of liquid limit,

while the Injana Formation showed the lowest percentage. Specifically, in the Fatha Formation, the liquid limit ranged from 27 to 43%, with an average of 31.88 percent, whereas in the Injana Formation, it ranged from 18 to 34.8%, with an average of 30.42%. These results indicate that samples from the Fatha Formation generally had a higher liquid limit compared to samples from the Injana Formation.

The plastic limit, representing the moisture content at which soil transitions from a plastic to a semisolid state, ranged from 16 to 22%, with an average of 19%. Notably, there was a small difference in the plastic limit between the Fatha Formation (average of 19.46%) and the Injana Formation (average of 19.35%).

The plasticity index, which is the difference between the liquid limit and the plastic limit, varied from 2 to 21%. The majority of the samples exhibited a plasticity index ranging from 5 to 20%, indicating a transition from low plasticity to medium plasticity. It is worth noting that the presence of a significant percentage of silt in most soil samples contributed to the plasticity index falling within the low to medium range.

Partial Analysis of the Soil Using IDW

Using the IDW approach, the spatial distribution of physical properties was examined, leading to the identification of five

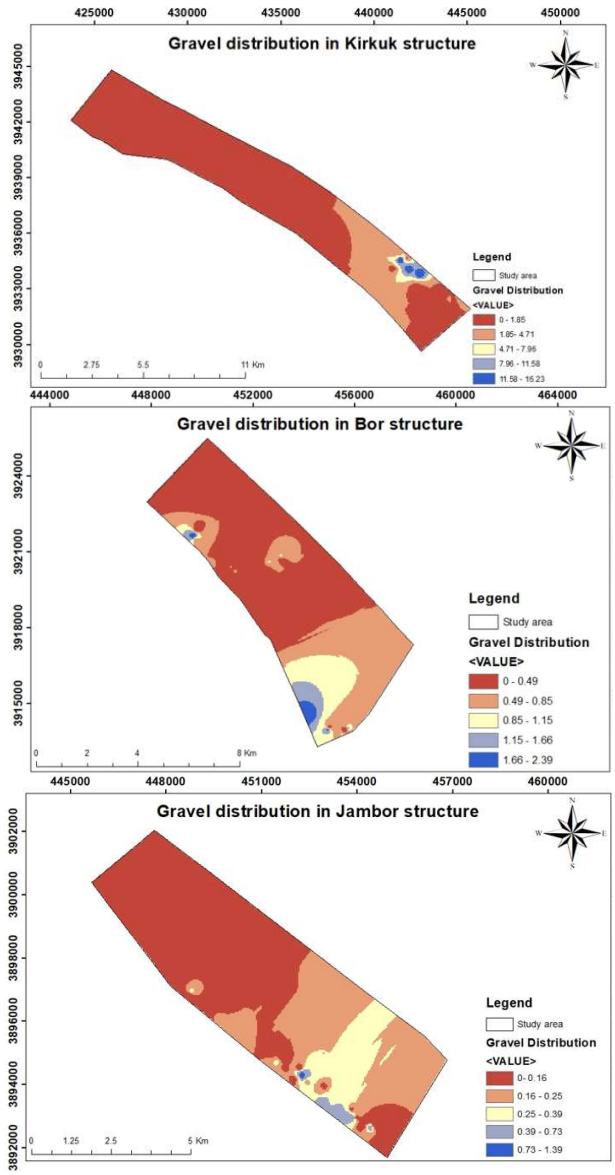

Fig. 3: IDW representation of gravel.

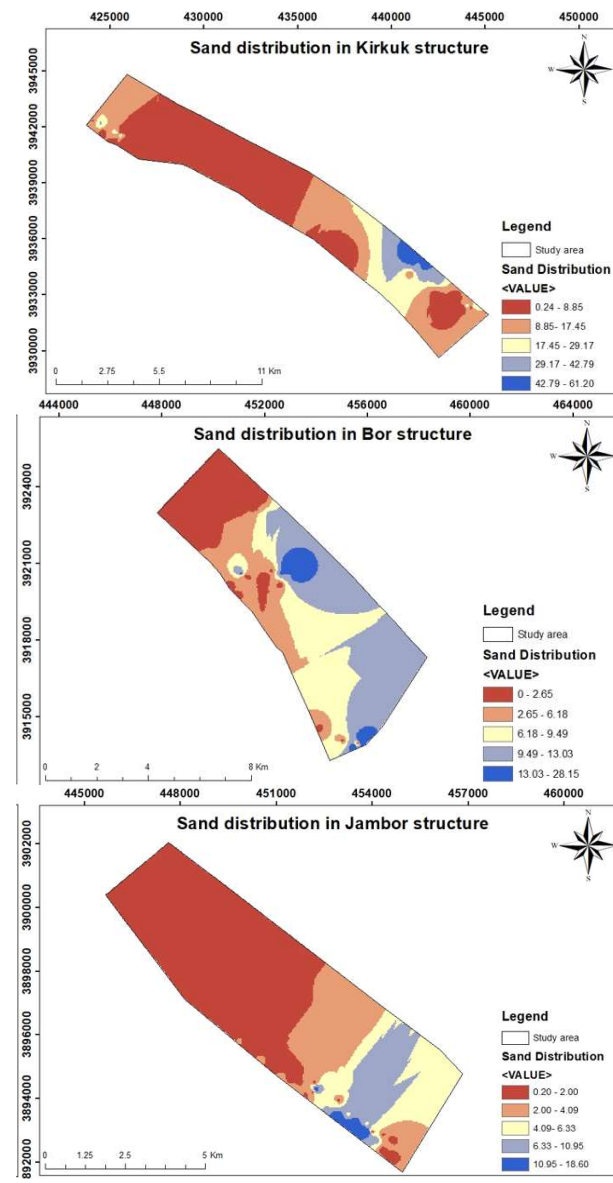

Fig. 4: IDW representation of sand.

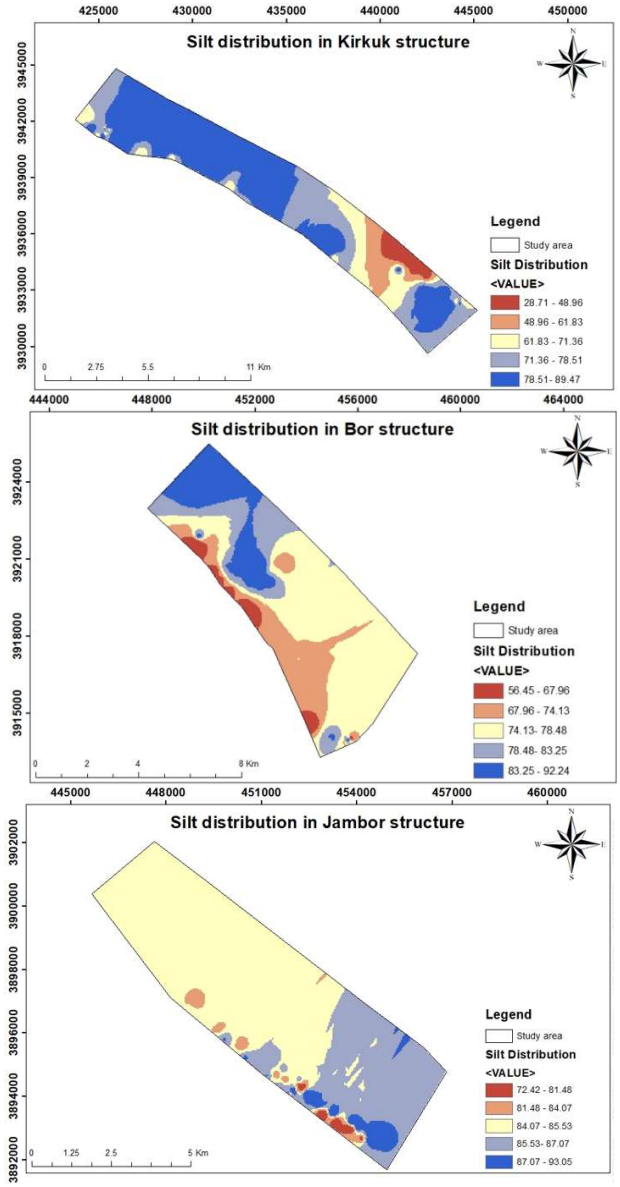

Fig. 5: IDW representation of silt.

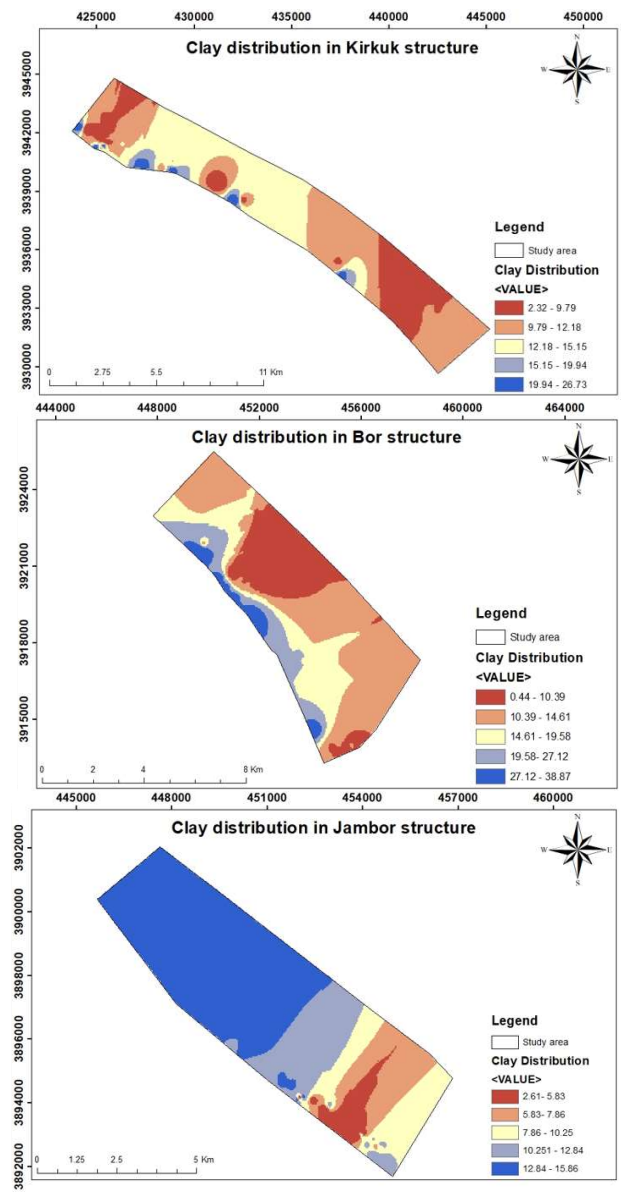

Fig. 6: IDW representation of clay.

distinct regions: very low, low, medium, high, and very high. Higher-proportion regions are represented in blue, while lower-proportion regions are depicted in red. The study area was divided into three sections: Kirkuk structure, Bor structure, and Jambor structure. Kirkuk structure (ranging from 28.71 to 89.47%), Bor structure (ranging from 56.45 to 92.24%), and Jambor structure (ranging from 72.42 to 93.05%), as depicted in Fig. 5, were all found to contain a comparatively high proportion of silt. Fig. 3 provides insights into the distribution of gravel percentages across the three sections, showing a range of 0 to 16.23% in the Kirkuk structure, 0 to 2.39% in the Bor structure, and 0 to 1.39% in the Jambor structure.

Similarly, Fig. 4 showcases the variation in sand percentages, with the Kirkuk structure ranging from 0.24 to 61.20%, the Bor structure ranging from 0.0 to 28.15%, and the Jambor structure ranging from 0.2 to 18.6%. The percentage of clay is depicted in Fig. 6, revealing a range of 2.32 to 26.73% in the Kirkuk structure, 0.44 to 38.87% in the Bor structure, and 2.61 to 15.86% in the Jambor structure. Field measurements utilizing an HS-5001EZ moisture-density gauge were conducted to determine the dry density

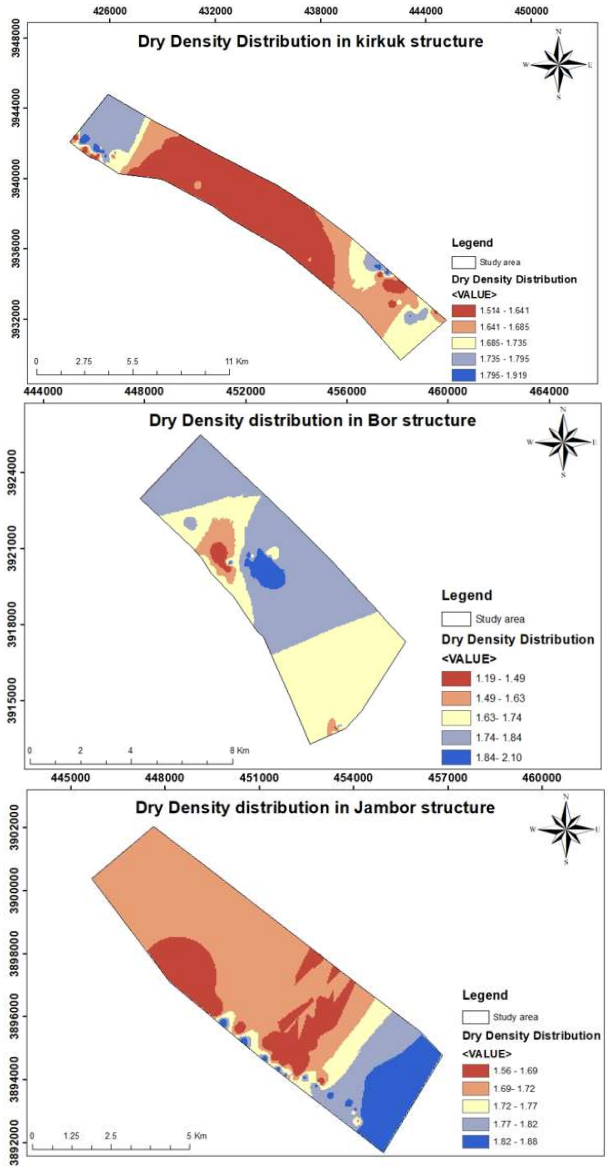

Fig. 7: IDW representation of dry density.

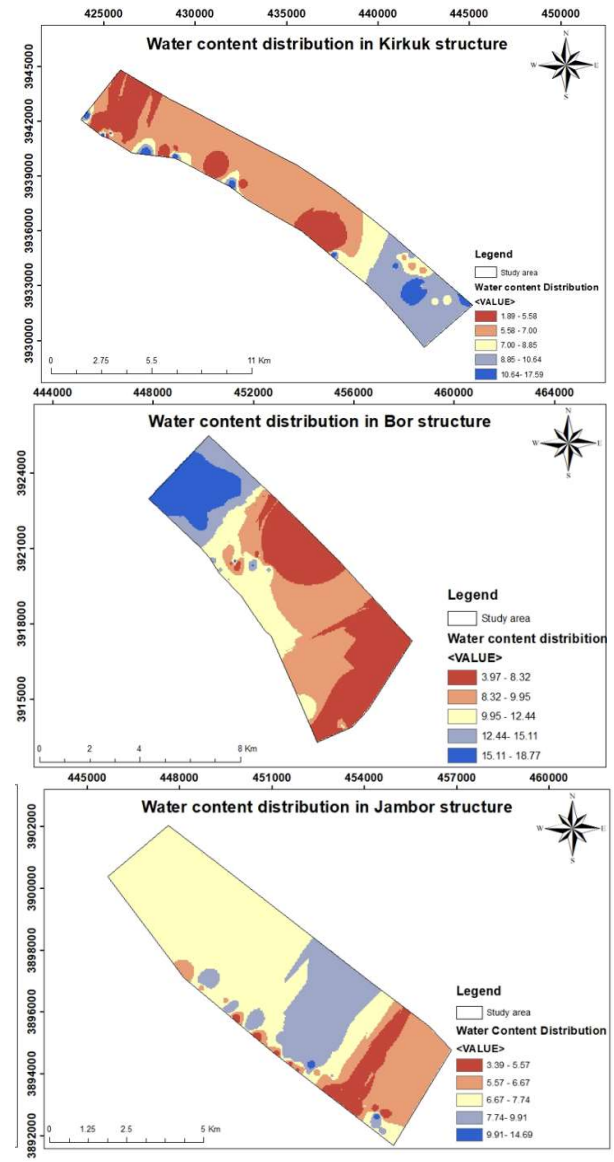

Fig. 8: IDW representation of water content.

Table 1: The root mean squared error (RMSE) and R^2 for maps.

Physical properties	Kirkuk hills		Bor mountain		Jambor hills	
	RMSE	R^2	RMSE	R^2	RMSE	R^2
Water Content	0.078	0.825	0.087	0.815	0.066	0.83
Dry density	0.015	0.891	0.0054	0.858	0.0033	0.92
Liquid Limit	0.29	0.765	0.098	0.8	0.15	0.79
Plastic Limit	0.16	0.78	0.047	0.858	0.044	0.863
Specific gravity	0.022	0.884	0.0044	0.92	0.00096	0.945
Gravel	0.038	0.865	0.012	0.9	0.028	0.877
Sand	0.123	0.793	0.093	0.81	0.079	0.82
Silt	0.21	0.775	0.059	0.85	0.113	0.798
Clay	0.065	0.841	0.046	0.86	0.059	0.85

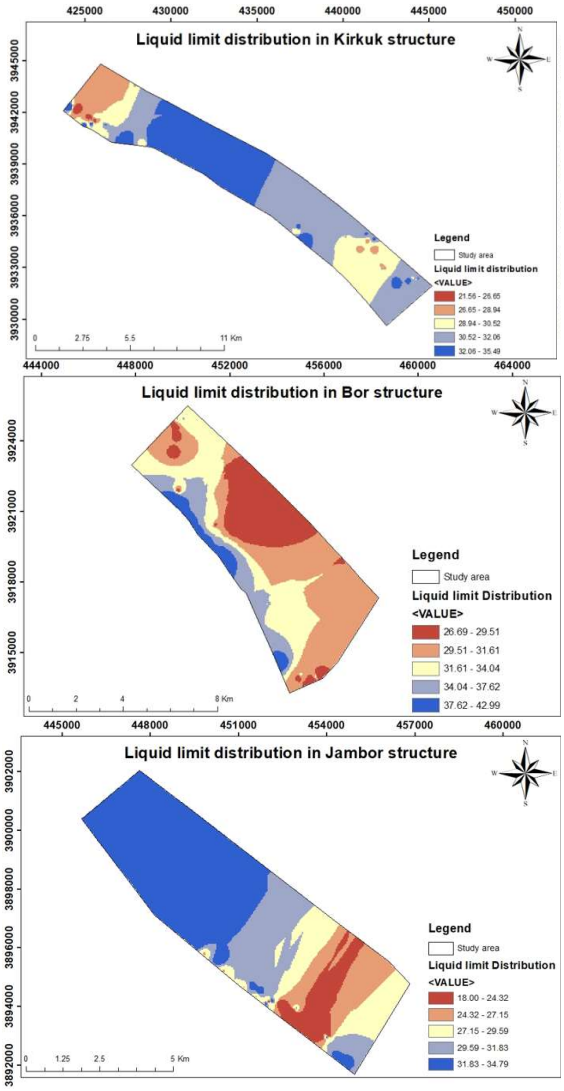

Fig. 9: IDW representation of liquid limit.

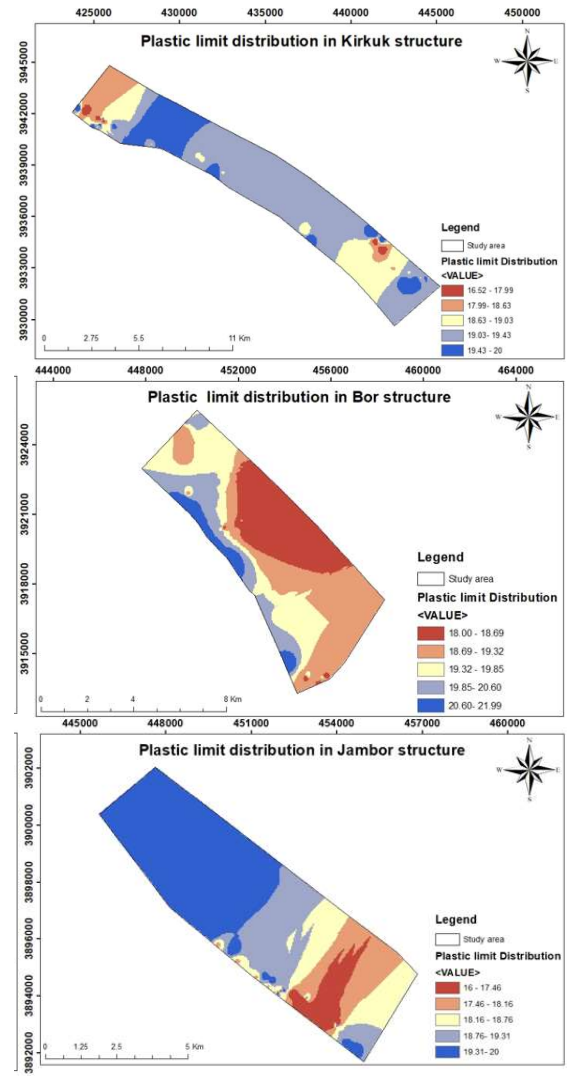

Fig. 10: IDW representation of plastic limit.

Table 2: Relationship between the physical properties of red clay.

	Water content	Dry Density	Liquid Limit	Plastic Limit	Plasticity index	specific gravity	Gravel	sand	silt	clay
Water content	1									
Dry Density	0.06	1								
Liquid Limit	0.112	0.08	1							
Plastic Limit	0.12	0.08	0.94	1						
Plasticity index	0.09	0.07	0.99	0.89	1					
specific gravity	0.151	0.012	0.102	0.006	0.009	1				
Gravel	0.003	0.013	0.00007	0.00005	0.0002	0.01	1			
sand	0.007	0.001	0.04	0.03	0.036	0.018	0.33	1		
silt	0.002	0.006	0.03	0.03	0.031	0.0013	0.45	0.81	1	
clay	0.09	0.003	0.58	0.495	0.596	0.151	0.005	0.07	0.02	1

and water content, as shown in Fig. 7 and Fig. 8, respectively. Dry density values ranged from 1.51 to 1.92 g.m^{-3}, in the Kirkuk structure, 1.19 to 2.10 g.m^{-3} in the Bor structure, and 1.56 to 1.88 g.m^{-3} in the Jambor structure.

Water content varied between 1.89 and 17.59% in the Kirkuk structure, 3.97 and 18.77% in the Bor structure, and 3.39 and 14.69% in the Jambor structure. Fig. 9, 10, and 11 show the range of Atterberg limits in the soil analysis. Fig. 9 provides insights into the liquid limit, which spans from 18 to 43. Fig. 10 presents the plastic limit, ranging from 16 to 22. The plasticity index, displayed in Fig. 11, varies from 4 to 21. It is worth noting that a substantial proportion of soil samples contain silt, resulting in a plasticity index that predominantly falls within the low to medium range.

Validation and Model Generation

To validate the accuracy of the physical property maps generated using the IDW method for red clay, a validation process was conducted. A subset of 30% of the soil samples was utilized to compare the field measurements with the values estimated by the IDW interpolation. Table 1 provides the Root Mean Square Error (RMSE) values for the various physical properties assessed during the validation process. Choosing an interpolation method depends on the size of the data present in a study area. Different interpolation methods were applied to choose the best method and apply it to producing maps of the physical and chemical properties of red clay. The accuracy of the maps was calculated by applying the root mean square. The IDW method was the most accurate and appropriate method to produce maps. R^2 of the IDW ranged between 0.74 and 0.92, while R^2.

A linear regression model was employed to establish connections and characterize the physical characteristics

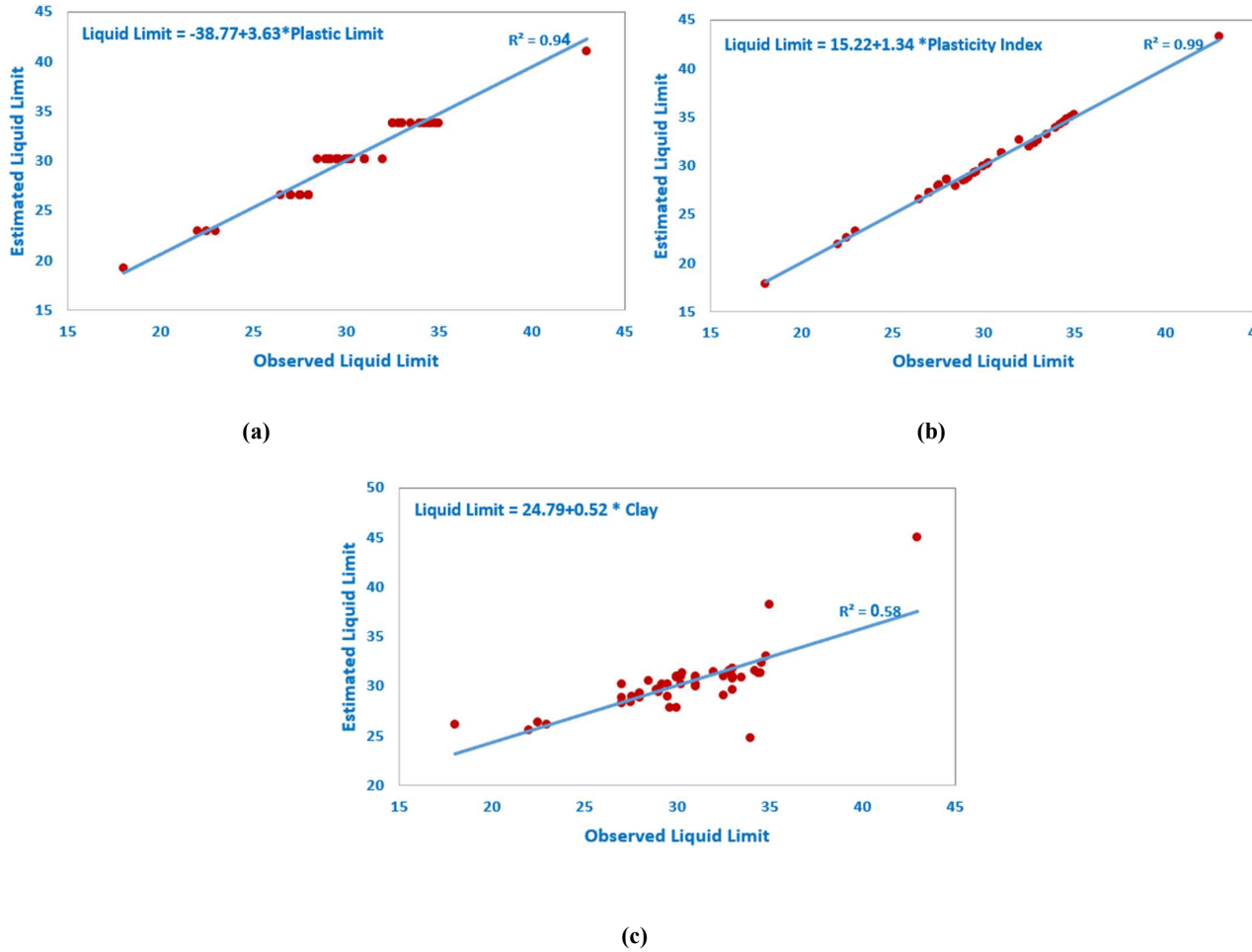

Fig. 11: Correlation Liquid Limit with (a) Plastic Limit, (b) Plasticity Index, and (c) Clay.

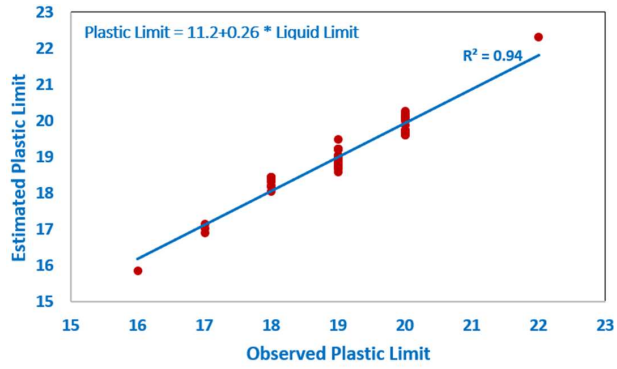

(b)

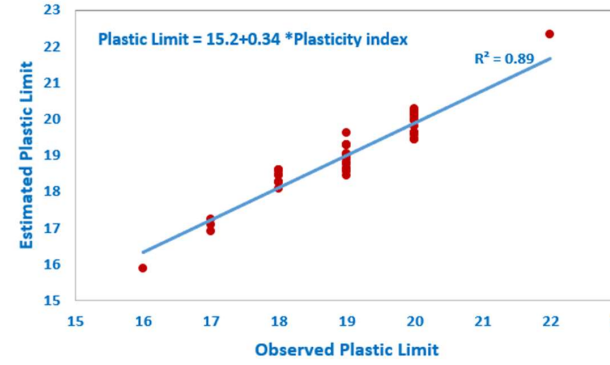

(a)

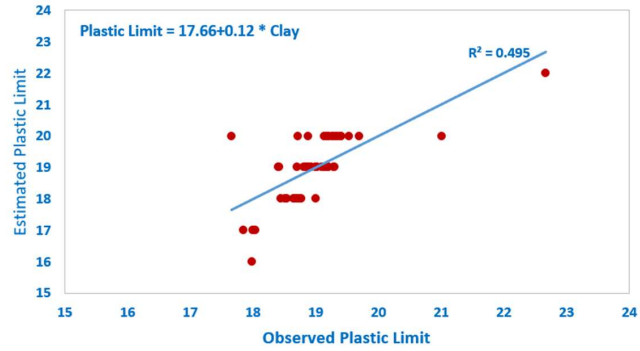

(c)

Fig. 12: Correlation of Plastic Limit with (a) Liquid limit, (b) Plasticity Index, and (c) Clay.

of red clay. The relationships between various soil properties, including soil texture (gravel, sand, silt, and clay), Atterberg limits (liquid limit, plastic limit, and plasticity index), water content, dry density, and specific gravity, were examined. The correlation analysis results are presented in Table 2.

The correlation analysis revealed a weak positive association between water content and liquid limit, plastic limit, and specific gravity, with correlation coefficients of 0.12, 0.120, and 0.151, respectively. However, no significant relationship was observed between dry density and the other parameters.

Regarding the liquid limit, a strong positive correlation was found with the plastic limit and plasticity index (0.94 and 0.99, respectively), a moderately positive correlation with clay content (0.58), and a weak positive correlation with specific gravity (0.102). The plastic limit exhibited a moderately significant association with clay content (0.495), while a high positive correlation was observed between the plasticity index and plastic limit (0.89). Furthermore, an intermediate positive association (0.596) was found between the plasticity index and clay percentage. The clay content showed only a slight positive correlation with specific gravity (0.151). Gravel displayed a moderately favorable association with sand (0.33) and silt (0.45), which is a common trend. Notably, a strong positive correlation (0.81) was identified between sand and silt percentages. The correlations between liquid limit, plastic limit, and plasticity index exhibit a direct and ideal correlation. The logical nature of these interactions arises from their dependence on common elements, such as clay content.

Figs. 11 to 16 display examples of correlation coefficients and regression equations obtained through the linear regression model. These figures, calculated using ArcMap software, demonstrate the relationships between the investigated soil parameters. The correlation coefficients,

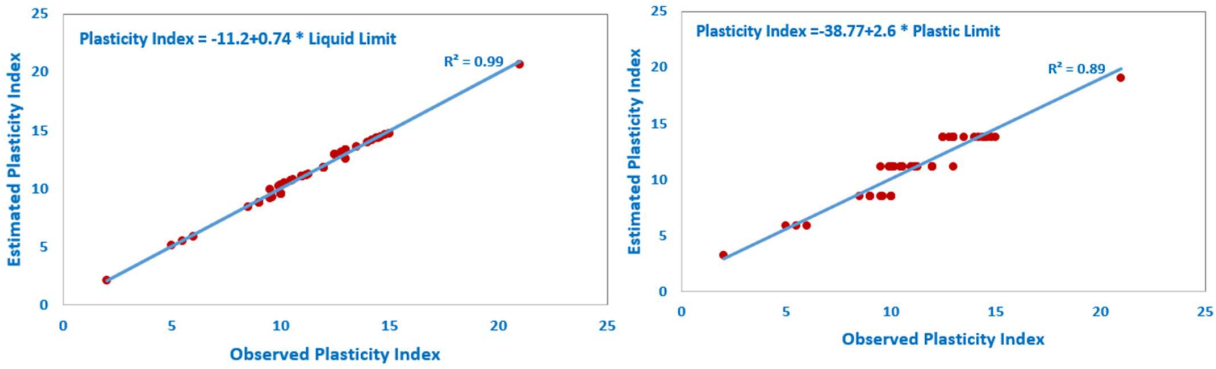

(a) (b)

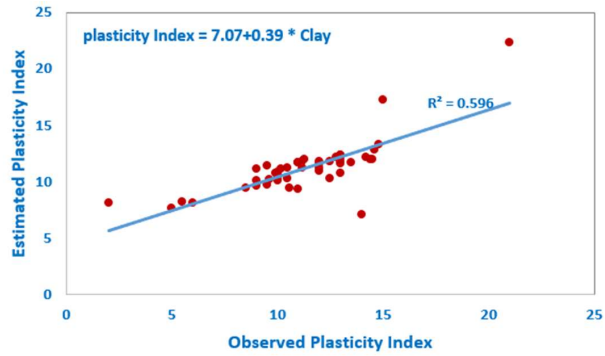

(c)

Fig. 13: Correlation of Plasticity Index with (a) Liquid limit, (b)Plastic Limit, and (c)Clay.

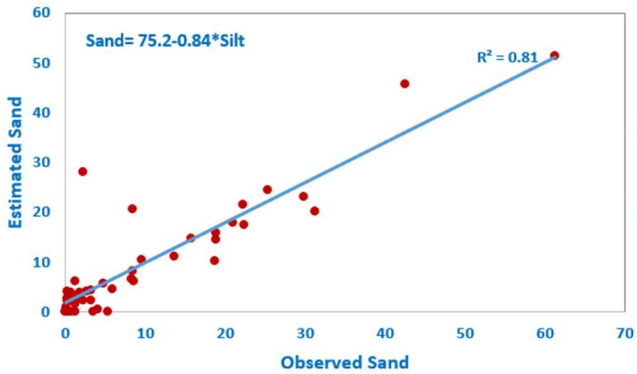

Fig. 14: Correlation of sand with silt.

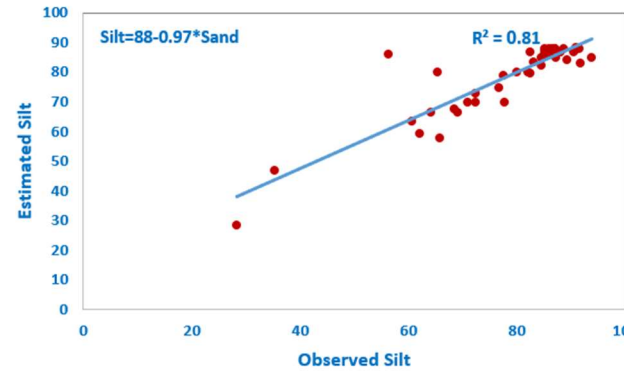

Fig. 15: Correlation of silt with sand.

represented by the R-value, indicate the strength and direction of the associations. The empirical regression equations derived from the model offer initial insights into the characteristics of the studied variables.

CONCLUSION

The analysis of red clay's physical parameters using the IDW approach and linear regression modeling, covering an area of 268.12 km2 and three different structures (Kirkuk,

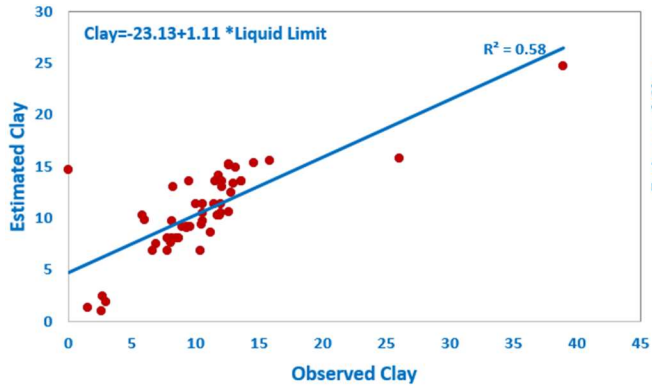

(a)

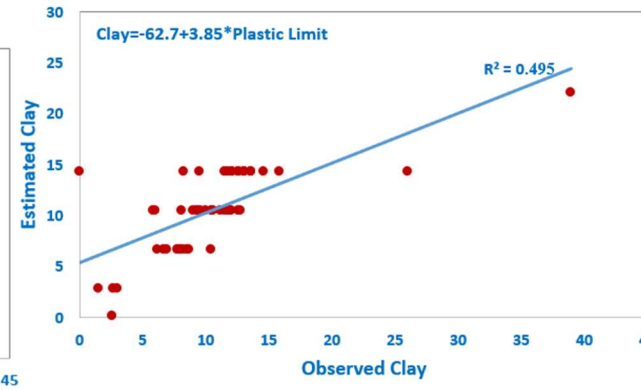

(b)

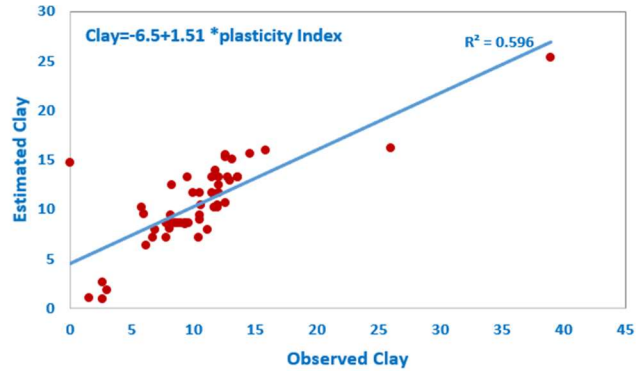

(c)

Fig. 16: Correlation of Clay with (1) Liquid limit, (2) Plastic Limit, and (c) Plasticity Index.

Bor, and Jambor), has yielded significant insights into the characteristics of the soil. By examining soil samples from 52 locations and combining laboratory data with IDW and regression results, several key findings have emerged.

First, the IDW method coupled with linear regression has proven to be a rapid, cost-effective, and reliable approach for obtaining soil property data. This approach enables the creation of accurate digital maps of red clay's physical features. Regarding the soil texture analysis, silt concentration exhibited the widest range, varying from 28.56% to 92.28%. On the other hand, gravel content was found to be relatively low, ranging from 0% to 16.03%. These findings highlight the dominance of silt in the soil composition.

The field measurements conducted using the HS-5001EZ moisture-density gauge revealed water content ranging from 2.24% to 18.8%, while dry density values ranged from 1.19 to 2.12. These results provide insights into the soil's moisture characteristics and density distribution across the study area.

The analysis of Atterberg limits demonstrated a range of 21 to 43 for the liquid limit and 16 to 22 for the plastic limit. These limits indicate the soil's consistency and behavior in response to moisture content. Furthermore, the plasticity index, reflecting the soil's plasticity, fell within the low to medium range due to the significant percentage of silt present in most soil samples.

The linear regression model revealed positive correlations between the liquid limit, plastic limit, and plasticity index, with Pearson's correlation coefficients of 0.94 and 0.99, respectively. Additionally, the liquid limit displayed a

moderately positive relationship with clay content (R = 0.58) and a weak positive association with specific gravity ($R^2 = 0.12$). The plastic limit and plasticity index exhibited a positive correlation with clay concentration ($R^2 = 0.495$ and $R^2 = 0.596$, respectively).

Interestingly, no correlation was found between dry density and other physical variables, suggesting that dry density is independent of the measured parameters. Furthermore, a stronger relationship was observed between clay content and the plastic limit compared to the liquid limit. Moreover, the liquid limit, plastic limit, and specific gravity were all weakly positively correlated with water content, indicating the influence of moisture on these parameters.

Last, gravel showed a moderate positive correlation with sand and silt concentrations. Additionally, a strong positive correlation ($R^2 = 0.81$) was observed between sand and silt contents, indicating their close association with the soil composition.

In summary, the comprehensive analysis of red clay's physical properties using the IDW method and linear regression modeling has provided valuable insights into the soil's characteristics. These findings enhance our understanding of the soil composition, moisture characteristics, and behavior, contributing to effective soil management and land-use planning in the study area.

REFERENCES

Akumu, C., Johnson, J., Etheridge, D., Uhlig, P., Woods, M., Pitt, D. and McMurray, S. 2015. GIS-fuzzy logic-based approach in modeling soil texture: using parts of the Clay Belt and Hornepayne region in Ontario Canada as a case study. Geoderma, 239: 13-24.

Al-Naqib, K.M. 1959. Geology of Southern Area of Kirkuk Liwa, Iraq. General Secretariat of the League of Arab States, Cairo, Egypt.

Alhirmizy, S. 2015. Automatic mapping of lineaments using shaded relief images derived from Digital Elevation Model (DEM) in Kirkuk Northeast Iraq. Int. J. Sci. Res., 4(5): 2228-2233.

Belief, E. 2018. GIS based spatial modeling to mapping and estimation relative risk of different diseases using inverse distance weighting (IDW) interpolation algorithm and evidential belief function (EBF) (Case study: Minor Part of Kirkuk City, Iraq). Int. J. Eng. Technol., 7(4.37): 185-191.

Buday, T. 1980. The Regional Geology of Iraq: Stratigraphy and Paleogeography. Dar El-Kutib Publication House, University of Mosul, Baghdad, p. p445.

Buenemann, M., Coetzee, M.E., Kutuahupira, J., Maynard, J.J. and Herrick, J.E. 2023. Errors in soil maps: The need for better on-site estimates and soil map predictions. PloS One, 18(1): e0270176.

da Silva Chagas, C., de Carvalho Junior, W., Bhering, S.B. and Calderano Filho, B. 2016. Spatial prediction of soil surface texture in a semiarid region using random forest and multiple linear regressions. Catena, 139: 232-240.

Eskandari, M., Zeinadini, A., Seyedmohammadi, J. and Navidi, M. 2023. Estimating quantity of date yield using soil properties by regression and artificial neural network. Commun. Soil Sci. Plant Anal., 54(1): 36-47.

Fongaro, C.T., Demattê, J.A., Rizzo, R., Lucas Safanelli, J., Mendes, W. d. S., Dotto, A.C., Vicente, L.E., Franceschini, M.H. and Ustin, S.L. 2018. Improvement of clay and sand quantification based on a novel approach with a focus on multispectral satellite images. Remote Sens., 10(10): 1555.

Jabbar, M.F.A. 2015. Geomorphology and Morphometry of Segmented Kirkuk Alluvial Fan, Northern Iraq. Iraqi Bull. Geol. Min., 11(2): 27-43.

Jaber, H.S., Shareef, M.A. and Merzah, Z.F. 2022. Object-based approaches for land use-land cover classification using high resolution quick bird satellite imagery (a case study: Kerbela, Iraq). Geod. Cartogr., 48(2): 85-91-85-91.

Jassim, S.Z. and Goff, J.C. 2006. Geology of Iraq. DOLIN, sro, distributed by Geological Society of London.

Liao, K., Xu, S., Wu, J. and Zhu, Q. 2013. Spatial estimation of surface soil texture using remote sensing data. Soil Sci. Plant Nutr., 59(4): 488-500.

Maarez, H.G., Jaber, H.S. and Shareef, M.A. 2022. Utilization of Geographic Information System for hydrological analyses: A case study of Karbala province, Iraq. Iraqi J. Sci., 4118-4130.

Martins, A.K. and Gadiga, B.L. 2015. Satellite remote sensing for mineral deposit assessment of clay in Mubi Local Government Area of Adamawa State, Nigeria. Geosci., 5(1): 26-30.

Mezaal, M.R. and Pradhan, B. 2018. An improved algorithm for identifying shallow and deep-seated landslides in dense tropical forest from airborne laser scanning data. Catena, 167: 147-159.

Mezaal, M.R., Pradhan, B. and Rizeei, H.M. 2018. Improving landslide detection from airborne laser scanning data using optimized Dempster–Shafer. Remote Sens., 10(7): 1029.

Mezaal, M.R., Pradhan, B., Sameen, M.I., Mohd Shafri, H.Z. and Yusoff, Z.M. 2017a. Optimized neural architecture for automatic landslide detection from high-resolution airborne laser scanning data. Appl. Sci., 7(7): 730.

Mezaal, M.R., Pradhan, B., Shafri, H.Z.M. and Yusoff, Z.M. 2017b. Automatic landslide detection using Dempster–Shafer theory from LiDAR-derived data and orthophotos. Geomat., Nat. Hazards Risk, 8(2): 1935-1954.

Mohamed, E., Ali, A., El-Shirbeny, M., Abutaleb, K. and Shaddad, S.M. 2020. Mapping soil moisture and their correlation with crop pattern using remotely sensed data in arid regions. Egypt. J Remote Sens. Space Sci., 23(3): 347-353.

Muhaimeed, A.S. and Al-Hedny, S. 2013. Evaluation of long-term vegetation trends for northeastern Iraq: Mosul, Kirkuk, and Salah al-Din. IOSR J. Agric. Veter. Sci., 5(2): 67-76.

Nistor, M.M., Rahardjo, H., Satyanaga, A., Hao, K.Z., Xiaosheng, Q. and Sham, A.W.L. 2020. Investigation of groundwater table distribution using borehole piezometer data interpolation: Case study of Singapore. Eng. Geol., 271: 105590.

Raheem, A.M., Naser, I.J., Ibrahim, M.O. and Omar, N.Q. 2023. Inverse distance weighted (IDW) and kriging approaches integrated with linear single and multi-regression models to assess particular physical-consolidation soil properties for Kirkuk city. Model. Earth Syst. Environ., 72: 4080

Raheem, A.M. and Omar, N.Q. 2021. Investigation of distinctive physico-chemical soil correlations for Kirkuk city using spatial analysis technique incorporated with statistical modeling. Int. J. Geo-Eng., 12(1): 1-21.

Raheem, A.M., Omar, N.Q., Naser, I.J. and Ibrahim, M.O. 2022. GIS implementation and statistical analysis for significant characteristics of Kirkuk soil. J. Mech. Behav. Mater., 31(1): 691-700.

Ratshiedana, P.E., Abd Elbasit, M.A., Adam, E., Chirima, J.G., Liu, G. and Economon, E.B. 2023. Determination of soil electrical conductivity and moisture on different soil layers using electromagnetic techniques in irrigated arid environments in South Africa. Water, 15(10): 1911.

Sahbeni, G., Ngabire, M., Musyimi, P.K. and Székely, B. 2023. Challenges and opportunities in remote sensing for soil salinization mapping and

monitoring: A review. Remote Sens., 15(10): 2540.
Shahien, M. and Ogila, W.A. 2022. Prediction of geotechnical properties of deltaic clays by using regression analysis models. Egypt. J. Pure Appl. Sci., 59(2): 36-62.
Shareef, M., Hassan, N., Hasan, S. and Khenchaf, A. 2020. Integration of sentinel-1A and sentinel-2b data for land use and land cover mapping of the Kirkuk Governorate, Iraq. Int. J. Geoinform., 16(3).
Shareef, M.A. and Hasan, S.F. 2020. Characterization and estimation of date palm trees in an urban area using GIS-based least-squares model and minimum noise fraction images. J. Ecol. Eng., 21(6).
Shareef, M.A., Toumi, A. and Khenchaf, A. 2014. Estimation of water quality parameters using the regression model with fuzzy k-means clustering. Int. J. Adv. Comput. Sci. Appl., 5(6).
Shit, P.K., Bhunia, G.S. and Maiti, R. 2016. Spatial analysis of soil properties using GIS based geostatistics models. Model. Earth Syst. Environ., 2(2): 1-6.
Sridevy, S., Raj, M.N., Kumaresan, P., Balakrishnan, N., Tilak, M., Raj, J. and Rani, P. 2023. Mapping of soil properties using machine learning techniques. Int. J. Environ. Clim. Change, 13(8): 684-700.
Taqi, A.H., Al Nuaimy, Q.A. and Karem, G.A. 2016. Study of the properties of soil in Kirkuk, Iraq. J. Radiat. Res. Appl. Sci., 9(3): 259-265.
Yadav, T., Singh, Y., Yadav, S.S., Singh, A. and Patel, T. 2023. Spatial variability in soil properties, delineation site-specific management division based on soil fertility using fuzzy clustering in Gwalior, Madhya Pradesh, India. Int. J. Plant Soil Sci., 35(6): 49-78.
Yang, L., Kaisheng, C., Mengfei, L. and Yingchao, W. 2020a. Study on failure of red clay slopes with different gradients under dry and wet cycles. Bull. Eng. Geol. Environ., 79(9): 4609-4624.
Yang, W., Zhao, Y., Wang, D., Wu, H., Lin, A. and He, L. 2020b. Using principal components analysis and IDW interpolation to determine spatial and temporal changes of surface water quality of Xin'anjiang river in Huangshan, China. Int. J. Environ. Res. Public Health, 17(8): 2942.
Zhang, Y., Pu, S., Li, R.Y.M. and Zhang, J. 2020. Microscopic and mechanical properties of undisturbed and remoulded red clay from Guiyang, China. Sci. Rep., 10(1): 1-14.
Zhu, A.-X., Qi, F., Moore, A. and Burt, J.E. 2010. Prediction of soil properties using fuzzy membership values. Geoderma, 158(3-4): 199-206.
Zolfaghari, Z., Mosaddeghi, M. and Ayoubi, S. 2015. ANN-based pedotransfer and soil spatial prediction functions for predicting Atterberg consistency limits and indices from easily available properties at the watershed scale in western Iran. Soil Use Manage., 31(1): 142-154.